Modeling and Analysis of a Thermoelectric-Assisted Two-Phase Condenser with Bidirectional Electro-Thermal Coupling

Andrés Hernández[a*], Geoffrey Roy[b], Mauricio Pedroza-Torres[a], Samuel Gendebien[a], Mathieu Delcroix[b], Pascal J. Jacques[b], Antoine de Ryckel[c] and Vincent Lemort[a]

*[a] Thermodynamics Laboratory, Université de Liège, Liège, Belgium, *e-mail: jahernandez@uliege.be*
[b] Institute of Mechanics, Materials, and Civil Engineering (iMMC – IMAP), Université catholique de Louvain, Louvain-la-Neuve, Belgium
[c] Calyos, Charleroi, Belgium

Abstract:
Two-phase thermal management systems such as heat pipes and mechanically pumped loops offer high heat transfer capability and compactness for energy and electronics cooling applications. More recently, integrating thermoelectric generators (TEGs) into condensation devices has emerged as a promising approach to combine heat rejection with low-grade power generation. However, most existing studies rely on experimental demonstrations or lumped thermal representations, limiting the understanding of the coupled thermo-hydraulic and electrical interactions governing such systems, particularly under two-phase flow conditions. This work presents a one-dimensional, spatially resolved model of a two-phase condenser equipped with an effective-property transverse thermoelectric generator (TTEG) wall. The framework resolves local heat transfer, pressure drop, phase evolution, and electrical response, while enabling bidirectional electro-thermal coupling between the condenser thermal field and the external electrical operating point. The model is analysed under three configurations: baseline operation without thermoelectric integration, open-circuit thermoelectric operation, and fully coupled electrical-load conditions. This formulation makes it possible to distinguish passive thermal effects associated with the thermoelectric wall from active current-dependent electro-thermal feedback, and to quantify how electrical loading influences phase distribution, heat transfer, and power generation. The results demonstrate that the proposed framework captures the dominant thermal and electrical interactions governing thermoelectric-assisted condensation, providing a physically consistent basis for identifying operating regimes where electro-thermal coupling may become more significant.

Keywords:
Two-phase condensation, Transverse thermoelectric generator (TTEG), Electro-thermal coupling, Segment-based modelling, Phase distribution, Heat transfer modification, Organic working fluids

1. Introduction

Two-phase thermal management systems, including heat pipes and pumped two-phase loops, are widely used in power electronics, aerospace thermal control, and industrial heat recovery due to their high heat transfer capacity and compactness [1]. In such systems, the condenser is responsible for heat rejection, directly affecting system stability, cycle efficiency, and working fluid inventory. Improving condenser performance while simultaneously recovering useful energy from rejected heat remains an important challenge in thermal system design.

Thermoelectric generators (TEGs) provide a solid-state means of converting temperature differences into electrical power [2]. Their operating principles, material requirements, and modelling approaches have been extensively reviewed for power generation and cooling applications [2, 3]. The integration of TEGs into heat exchangers has been explored in various configurations, including finned surfaces,

annular geometries, and heat pipe walls [4]. More recent studies have focused on embedding thermoelectric elements directly within heat exchanger structures, highlighting the influence of thermal resistance and operating conditions on overall performance [5–8]. Experimental studies confirm that thermoelectric-assisted heat exchangers can achieve simultaneous heat rejection and low-grade power generation, although at the expense of additional thermal resistance.

Among thermoelectric architectures, the Transverse Thermoelectric Generator (TTEG) offers specific advantages for tubular heat exchanger integration. Unlike conventional TEGs, where electrical current is aligned with the temperature gradient, TTEGs exploit the off-diagonal components of the Seebeck tensor in anisotropic composite laminates to generate a transverse voltage [9, 10]. By inclining alternating thermoelectric and metallic layers at an angle θ relative to the tube axis, a radial heat flux induces an axial electromotive force, enabling seamless tubular integration without discrete p–n junctions [11, 12]. Sakai et al. demonstrated that a tubular $Bi_{0.5}Sb_{1.5}Te_3$/Ni TTEG can deliver up to 2.5 W under an 83 K temperature difference across a 100 mm device [11], confirming the feasibility of this architecture for heat exchanger applications.

Despite these advances, most studies on thermoelectric-assisted heat exchangers rely on lumped or quasi-static thermal models [4, 7, 8, 13]. These approaches evaluate global performance assuming uniform temperature differences and therefore neglect spatial variations in thermodynamic and transport properties. While such simplifications may be acceptable in single-phase systems, they become limiting in two-phase condensers, where local heat transfer coefficients vary significantly between condensation and subcooled regions, and pressure drop continuously modifies saturation conditions and phase boundaries.

As a result, lumped approaches cannot resolve how a thermoelectric wall affects the spatial evolution of vapour quality, local heat transfer, phase boundaries, and electrical operating conditions along the condenser. They also prevent a clear distinction between passive thermal effects associated with thermoelectric integration and active electro-thermal interactions arising from electrical current flow.

To the best of the authors' knowledge, the local interaction between a transverse thermoelectric wall and two-phase condensation has not been investigated within a segment-resolved modelling framework. This work addresses this gap by developing a one-dimensional, segment-based model of a condenser with an integrated TTEG, in which heat transfer, pressure drop, phase evolution, and thermoelectric response are resolved along the tube length.

The proposed framework enables spatially resolved bidirectional electro-thermal coupling between the condenser thermal field and the electrical operating point. In contrast with lumped approaches, the model allows the system to be analysed under three distinct operating conditions: a baseline condenser without thermoelectric integration, an open-circuit thermoelectric configuration capturing passive thermal effects, and a fully coupled electrical-load condition including current-dependent Peltier and Joule effects. The objective is not to optimise the thermoelectric integration, but to establish a physically consistent modelling framework capable of isolating the dominant thermal and electrical interactions and identifying operating regimes where electro-thermal coupling becomes significant.

The remainder of the paper is organised as follows. Section 2. presents the modelling framework, including the thermo-hydraulic formulation, the TTEG model, and the coupling strategy. Section 3. defines the simulation setup and operating conditions. Section 4. reports the validation of the thermoelectric submodel against experimental data from Sakai et al. [11]. Section 5. discusses the results, and conclusions are drawn in Section 6..

2. Model Description

A one-dimensional, segment-resolved model is developed to describe the interaction between two-phase condensation and transverse thermoelectric power generation in a concentric tube condenser. The framework combines thermo-hydraulic, thermoelectric, and electrical submodels within a bidirectionally coupled formulation.

The modelling architecture is structured into three interacting layers, as illustrated in Fig. 1. Layer 1

describes the thermo-hydraulic behaviour of the condenser, resolving local heat transfer, pressure drop, and phase evolution. Layer 2 represents the transverse thermoelectric generator (TTEG) embedded in the condenser wall, where radial heat flux is converted into electrical power through effective anisotropic properties. Layer 3 describes the global electrical network, where segment-level electrical contributions are assembled in series and coupled to an external load.

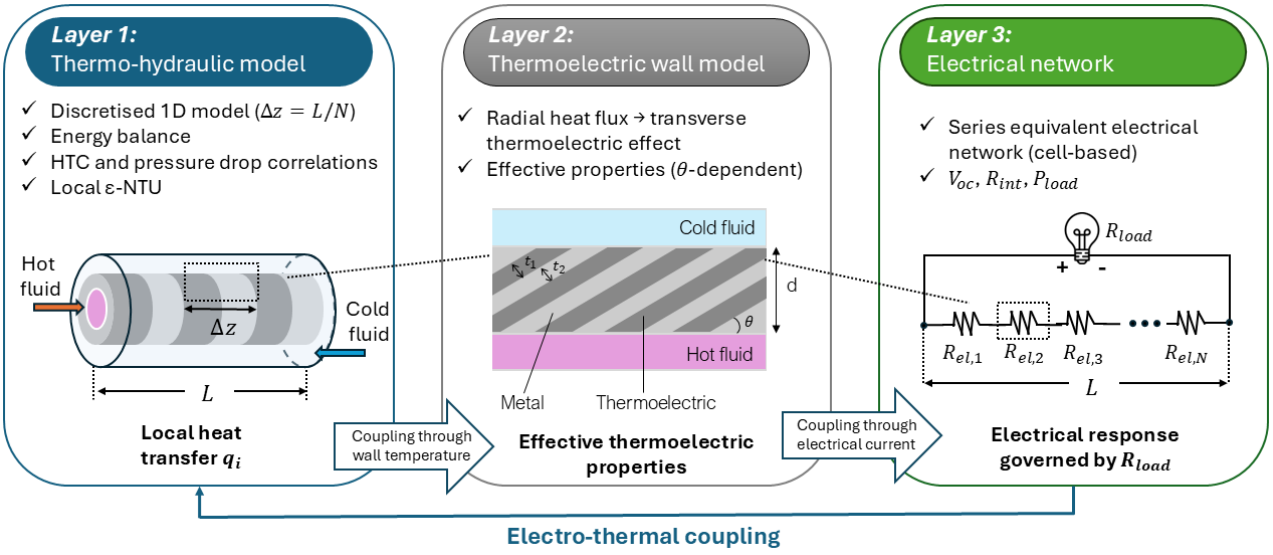

Figure 1: Three-layer modelling framework of the TTEG-integrated condenser: (1) thermo-hydraulic model, (2) thermoelectric wall model, and (3) electrical network. Bidirectional coupling links local heat transfer with global electrical generation.

The local heat flux determines the wall temperature field and therefore the thermoelectric response, while the resulting electrical current feeds back into the thermal behaviour through Peltier heat transport and Joule dissipation. To isolate passive and active effects, three configurations are considered: a baseline case with the thermoelectric wall disabled, an open-circuit thermoelectric case with $I = 0$, and a fully coupled case in which the current is determined by the external load.

2.1. Thermo-hydraulic framework

A steady-state one-dimensional model is developed for a concentric counter-current condenser, where R1233zd(E) condenses inside the inner tube while water flows in the annular region. The condenser of length L is discretized into N uniform segments:

$$\Delta z = \frac{L}{N} \tag{1}$$

Each segment is treated as a control volume and solved sequentially along the refrigerant flow direction.

Heat transfer coefficients.
The water-side heat transfer coefficient is evaluated from conventional internal-flow correlations based on the local Reynolds number,

$$Re_w = \frac{G_w D_h}{\mu_w} \tag{2}$$

where G_w is the water mass flux and D_h is the annular hydraulic diameter. For turbulent flow ($Re_w > 2300$), the Gnielinski correlation is used [14]:

$$Nu_w = \frac{(f/8)(Re_w - 1000)Pr_w}{1 + 12.7(f/8)^{1/2}(Pr_w^{2/3} - 1)} \tag{3}$$

On the refrigerant side, the local HTC depends on the thermodynamic phase. In two-phase regions, the condensation correlation proposed by Shah [15] is used, whereas single-phase liquid or vapour regions are evaluated using standard internal-flow correlations.

Overall heat transfer.
The local heat-transfer behaviour of segment i is represented by an equivalent cylindrical thermal-resistance network evaluated over the segment length Δz. The hot-side convective $R_{h,i}$, thermoelectric-wall conductive $R_{th,i}$, and cold-side convective $R_{c,i}$ resistances are combined into a total thermal resistance $R_{\mathrm{tot},i}$, from which the corresponding overall thermal conductance UA_i is obtained:

$$R_{\mathrm{tot},i} = R_{h,i} + R_{\mathrm{th},i} + R_{c,i}, \qquad UA_i = \frac{1}{R_{\mathrm{tot},i}} \tag{4}$$

The segment heat transfer rate is evaluated using the ε–NTU method [18]:

$$q_i^{\mathrm{NTU}} = \varepsilon_i C_{\min,i} \left(T_{\mathrm{ref},i} - T_{\mathrm{water},i}\right), \qquad NTU_i = \frac{UA_i}{C_{\min,i}} \tag{5}$$

where ε_i is the local heat-exchanger effectiveness obtained from the standard counter-current ε–NTU formulation.

Pressure drop and phase evolution.
The refrigerant phase is classified locally according to the segment enthalpy relative to saturation properties. The vapour quality is computed as:

$$x_i = \frac{h_i - h_f}{h_g - h_f} \tag{6}$$

In two-phase regions, the void fraction is evaluated using the correlation of Zivi [16], while the frictional pressure gradient is computed using the model of Friedel [17]. In single-phase regions, the pressure drop is evaluated with the Darcy–Weisbach equation:

$$\Delta P_i = f_i \frac{\Delta z}{D} \frac{G_i^2}{2\rho_i} \tag{7}$$

The refrigerant enthalpy and pressure are then updated as:

$$h_{i+1} = h_i - \frac{q_i}{\dot{m}_{\mathrm{ref}}}, \qquad P_{i+1} = P_i - \Delta P_i \tag{8}$$

2.2. Transverse thermoelectric wall model

The thermoelectric wall is modelled following the tubular transverse thermoelectric generator concept introduced by Kanno et al. [10] and experimentally applied to tubular geometries by Sakai et al. [11]. The TTEG consists of inclined thermoelectric and metallic layers, producing anisotropic effective transport properties. As a result, a radial temperature gradient induces an axial electromotive force through the off-diagonal Seebeck coefficient.
The effective Seebeck tensor is obtained by rotating the principal material tensor by the inclination angle θ. The transverse coefficient governing power generation is:

$$S_{\mathrm{eff}} = \left(S_{\parallel} - S_{\perp}\right) \sin\theta \cos\theta \tag{9}$$

where $S_{\parallel}$ and $S_{\perp}$ are the effective Seebeck coefficients parallel and perpendicular to the laminate direction, respectively.

Since the generated voltage develops along the axial direction of each segment, the circuit-level Seebeck coefficient is defined as:

$$S_{c,i} = \frac{\Delta z}{t_{\mathrm{th}}} S_{\mathrm{eff},i} \tag{10}$$

where $t_{\mathrm{th}} = r_o - r_i$ is the total radial thickness of the thermoelectric wall.
The radial thermal resistance of the cylindrical thermoelectric wall is:

$$R_{\mathrm{th},i} = \frac{\ln(r_o/r_i)}{2\pi k_{\mathrm{eff}} \Delta z} \tag{11}$$

where k_{eff} is the effective thermal conductivity, leading to the corresponding segment thermal conductance as:

$$G_{\mathrm{th},i} = \frac{1}{R_{\mathrm{th},i}} \tag{12}$$

The electrical resistance of segment i is expressed as:

$$R_{\mathrm{el},i} = \frac{L_{\mathrm{el},i}}{\sigma_{\mathrm{eff}} A_{\mathrm{el},i}} \tag{13}$$

where σ_{eff} is the effective electrical conductivity in the axial direction. The detailed evaluation of $S_{\parallel}$, $S_{\perp}$, k_{eff}, and σ_{eff} follows the anisotropic composite formulation reported by Kanno et al. [10].
For a given local thermal state, the heat transfer through the thermoelectric segment is evaluated from the equivalent local thermal-resistance network:

$$Q_{\mathrm{th},i} = \frac{T_{\mathrm{ref},i} - T_{\mathrm{water},i}}{R_{h,i} + R_{\mathrm{th},i} + R_{c,i}} \tag{14}$$

The corresponding junction temperatures are:

$$T_{h,i} = T_{\mathrm{ref},i} - Q_{\mathrm{th},i} R_{h,i}, \qquad T_{c,i} = T_{\mathrm{water},i} + Q_{\mathrm{th},i} R_{c,i} \tag{15}$$

The hot-side and cold-side heat rates are:

$$Q_{h,i} = Q_{\mathrm{th},i} + S_{\mathrm{c},i} I T_{h,i} - \frac{1}{2} I^2 R_{\mathrm{el},i}, \qquad Q_{c,i} = Q_{\mathrm{th},i} + S_{\mathrm{c},i} I T_{c,i} + \frac{1}{2} I^2 R_{\mathrm{el},i} \tag{16}$$

where the Peltier contribution acts at the thermoelectric junctions, while Joule dissipation is equally distributed between both sides.
The segment open-circuit voltage is:

$$V_{\mathrm{oc},i} = S_{\mathrm{c},i} \left(T_{h,i} - T_{c,i} \right) \tag{17}$$

The electrical power generated within each segment is therefore:

$$P_i = Q_{h,i} - Q_{c,i} = V_{\mathrm{oc},i} I - I^2 R_{\mathrm{el},i} \tag{18}$$

which ensures thermodynamic consistency between the thermal and electrical formulations.

2.3. Electro-thermal coupling

The interaction between the thermo-hydraulic model and the thermoelectric wall is formulated as a bidirectionally coupled nonlinear problem. For a given global current $I^{(k)}$ at outer iteration k, the unknown in segment i is the local heat duty q_i. The thermo-hydraulic model predicts a heat duty through the local ε–NTU formulation, while the thermoelectric model predicts the corresponding hot-side heat flux. Local consistency is enforced through:

$$r_i(q_i) = q_i^{\mathrm{NTU}}(q_i) - Q_{h,i}^{\mathrm{TE}}\left(q_i, I^{(k)}\right) = 0 \tag{19}$$

where q_i^{NTU} is the heat flux predicted by the thermo-hydraulic model and $Q_{h,i}^{\mathrm{TE}}$ is the hot-side heat flux obtained from the thermoelectric model.
The local residual is solved using a Newton–Raphson procedure:

$$q_i^{(m+1)} = q_i^{(m)} - \frac{r_i\left(q_i^{(m)}\right)}{\partial r_i / \partial q_i} \tag{20}$$

where m denotes the local Newton iteration. The Jacobian is evaluated numerically using finite differences:

$$\frac{\partial r_i}{\partial q_i} \approx \frac{r_i(q_i + \Delta q) - r_i(q_i)}{\Delta q} \tag{21}$$

The local iteration continues until:

$$|r_i| < \varepsilon_q \tag{22}$$

ensuring consistency between the thermo-hydraulic and thermoelectric descriptions of each segment before advancing to the next control volume.
After all segments are solved for $I^{(k)}$, the segment-level electrical contributions are assembled assuming a series connection:

$$V_{\mathrm{oc}}^{(k)} = \sum_{i=1}^{N} V_{\mathrm{oc},i}^{(k)}, \qquad R_{\mathrm{int}}^{(k)} = \sum_{i=1}^{N} R_{\mathrm{el},i}^{(k)} \tag{23}$$

The global electrical current is then updated through Ohm's law:

$$I^{(k+1)} = \frac{V_{\mathrm{oc}}^{(k)}}{R_{\mathrm{int}}^{(k)} + R_{\mathrm{load}}} \tag{24}$$

and the outer iteration continues until:

$$\left|I^{(k+1)} - I^{(k)}\right| < \varepsilon_I \tag{25}$$

At convergence, the electrical power delivered to the external load is consistent with both the circuit formulation,

$$P_{\mathrm{load}} = I^2 R_{\mathrm{load}} \tag{26}$$

and the thermoelectric energy conversion over all segments:

$$P_{\mathrm{load}} = \sum_{i=1}^{N} \left(Q_{h,i} - Q_{c,i}\right) \tag{27}$$

This equality provides a direct verification of the coupled solution and ensures electro-thermal consistency of the condenser model.

3. Simulation Setup

Two physical configurations are considered. The first reproduces the single-phase tubular TTEG experiments of Sakai et al. [11] and is used to validate the thermoelectric submodel independently of two-phase effects. The second corresponds to a concentric two-phase condenser operating with R1233zd(E), where the electro-thermal coupling is analysed under baseline, open-circuit, and fully coupled electrical-load conditions.

The validation case consists of a $Bi_{0.5}Sb_{1.5}Te_3$/Ni tubular TTEG under water–water conditions, with a prescribed temperature difference across the wall. The condenser case uses the same TTEG topology and material system, but extends the tube length to the condenser scale. Thermophysical properties of the working fluids are evaluated using CoolProp [19]. The main parameters are summarised in Table 1.

Table 1: Main parameters for the Sakai validation case and the two-phase condenser case.

Parameter	Symbol	Sakai validation	Condenser case	Unit
Geometry and TTEG parameters				
Inner-tube inner diameter	$D_{i,\mathrm{in}}$	10	10	mm
Inner-tube outer diameter	$D_{i,\mathrm{out}}$	14	14	mm
Thermoelectric wall thickness	t_{th}	2	2	mm
Outer-tube inner diameter	$D_{o,\mathrm{in}}$	20	20	mm
Tube length	L	110	400	mm
Number of segments	N	300	300	–
Inclination angle	θ	35	35	$^\circ$
Metal volume fraction	a	0.40	0.40	–
TE material / metal	–	BST / Ni	BST / Ni	–
Wall conductivity	k_{wall}	–	20	W/m·K
Operating conditions				
Working fluid	–	Water / Water	R1233zd(E) / Water	–
Hot-side inlet temperature	$T_{ref,\mathrm{in}}$	93	70	°C
Cold-side inlet temperature	$T_{water,\mathrm{in}}$	10	10	°C
Hot-side mass flow rate	$\dot{m}_{ref}$	333	4.0	g/s
Cold-side mass flow rate	$\dot{m}_{water}$	333	400	g/s
Inlet vapour quality	x_{in}	–	0.45	–
Flow arrangement	–	Parallel	Counterflow	–
Load resistance	R_{load}	varied	varied	Ω

For the condenser case, three operating modes are analysed: (i) baseline operation without thermoelectric integration, (ii) open-circuit thermoelectric operation with $I = 0$, and (iii) fully coupled operation with an external electrical load. This sequence separates the passive thermal resistance introduced by the TTEG wall from the active electro-thermal feedback induced by current flow.

Particular attention is given to the load resistance ratio R_L/R_{int}, which defines the electrical operating point. The load sweep combines logarithmic sampling over several decades with additional points near $R_L \approx R_{\mathrm{int}}$, including the exact matched-load condition, to identify the maximum power point and its thermal impact. Additional parametric studies vary the inlet vapour quality and refrigerant mass flow rate to assess their influence on the coupled behaviour.

The validation results are presented in Section 4., while the coupled condenser behaviour is discussed in Section 5..

4. Model Validation

In the absence of experimental data for the complete thermoelectric condenser, validation is restricted to the transverse thermoelectric submodel follow the parameters summarised in Section 3.. The objec-

tive is to assess whether the proposed TTEG formulation accurately reproduces the electrical response of a tubular transverse thermoelectric generator under controlled thermal conditions before its integration into the two-phase condenser framework.

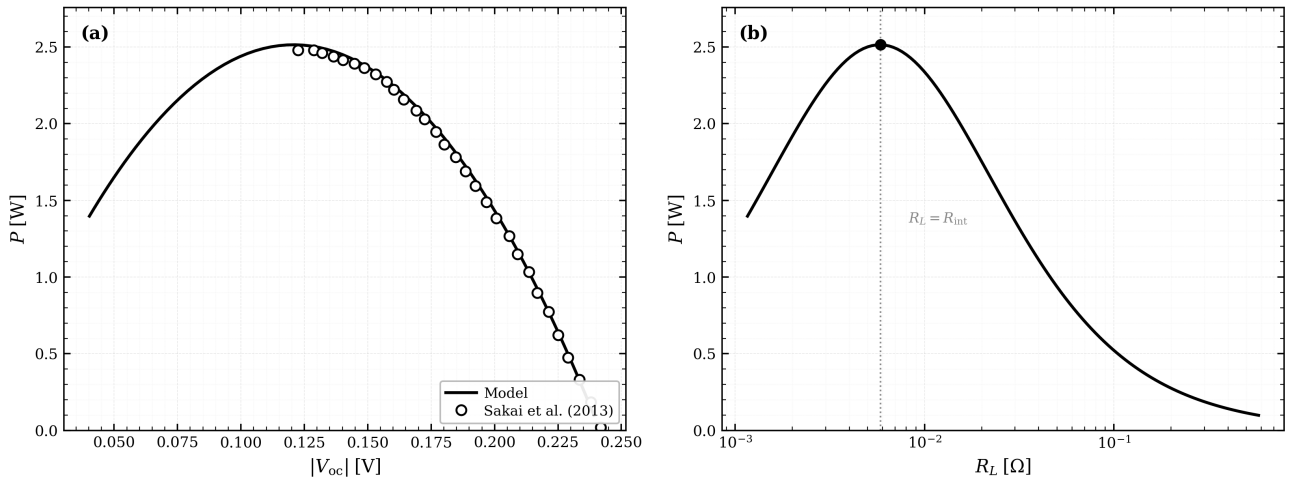

Figure 2: Validation of the transverse thermoelectric model against the experimental data of Sakai et al. [11]: **(a)** generated power as a function of voltage; **(b)** generated power as a function of load resistance.

Figure 2 compares the model predictions with digitised experimental data from Sakai et al. [11]. The model reproduces the characteristic parabolic power–voltage relationship and predicts a maximum power of approximately 2.5 W, in close agreement with the reported measurements.
The power–resistance curve further captures the expected impedance-matching behaviour, with the maximum power occurring near $R_L \approx R_{\text{int}}$, consistent with both thermoelectric theory and the experimental trend. This agreement supports the consistency of the effective property formulation and the load-dependent electrical closure.
Remaining deviations are attributed to the homogenised representation of the heterogeneous laminate, temperature-independent material properties, and uncertainties associated with data digitisation. Nevertheless, the agreement is sufficient for the present purpose, namely the integration of the validated TTEG formulation within the coupled two-phase condenser model.
The following sections therefore focus on the electro-thermally coupled condenser configuration.

5. Results and Discussion

5.1. Baseline condenser behaviour

The baseline configuration (TTEG disabled) defines the reference thermo-hydraulic behaviour of the condenser. The refrigerant enters as a two-phase mixture and undergoes progressive condensation followed by subcooling under counterflow conditions.
Figure 3 shows the axial evolution of refrigerant temperature, vapour quality, and local heat flux. In the two-phase region (shaded in blue), the temperature remains nearly constant at saturation while the vapour quality decreases monotonically, indicating latent heat-driven condensation. The transition to the subcooled region (shaded in beige) is marked by a temperature decrease and the disappearance of phase change.
The local heat flux decreases along the condenser due to the progressive reduction of the thermal driving force. Introducing the thermoelectric wall under open-circuit conditions ($I = 0$) produces a purely passive effect: the additional thermal resistance reduces the local heat flux, shifts the end of condensation downstream, and increases the outlet temperature.
When bidirectional coupling is activated, the electrical current further modifies the local thermal boundary conditions through Peltier and Joule effects. Although the generated electrical power re-

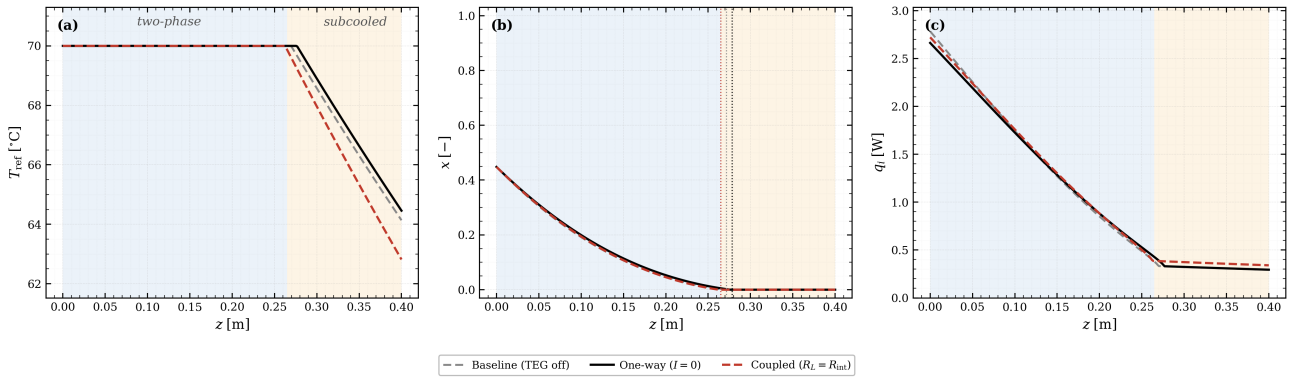

Figure 3: Axial profiles of refrigerant temperature, vapour quality, and local heat flux for baseline and TTEG configurations.

mains small compared with the condenser heat duty, these local electro-thermal interactions measurably affect the condensation length and phase distribution.

5.2. Electro-thermal coupling and load dependence

When bidirectional coupling is activated, the system behaviour becomes dependent on the electrical load resistance. Figure 4 shows the heat rates at the hot and cold sides of the thermoelectric wall (Q_h and Q_c), together with the electrical load power and system efficiency, as a function of the load ratio R_L/R_{int}.

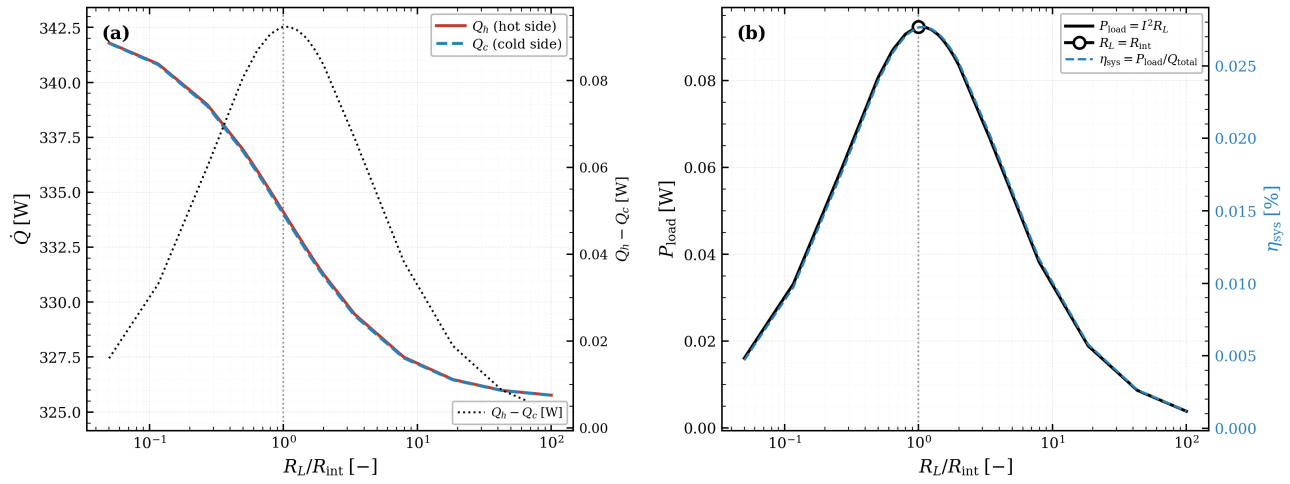

Figure 4: Electro-thermal coupling as a function of load resistance ratio: (a) heat rates at the thermoelectric wall; (b) electrical load power and system efficiency $\eta_{\text{sys}} = P_{\text{load}}/Q_{\text{total}}$.

The electrical power delivered to the load satisfies:

$$P_{\text{load}} = I^2 R_L = Q_h - Q_c \tag{28}$$

providing direct consistency between the electrical and thermal formulations.
The maximum electrical power is approximately 0.09 W, whereas the condenser heat duty is of the order of 3.3×10^2 W. Consequently, the system efficiency reaches only $\eta_{\text{sys}} \approx 0.027\%$.
The electrical power follows the expected impedance-matching behaviour, reaching a maximum near $R_L/R_{\text{int}} = 1$. For $R_L \gg R_{\text{int}}$, the current tends to zero and the coupled solution approaches the passive open-circuit thermoelectric case.

5.3. Impact on condenser thermal performance

The electrical operating point directly affects the global condenser performance. Figure 5 shows the evolution of the total heat duty and refrigerant outlet temperature as a function of R_L/R_{int}.

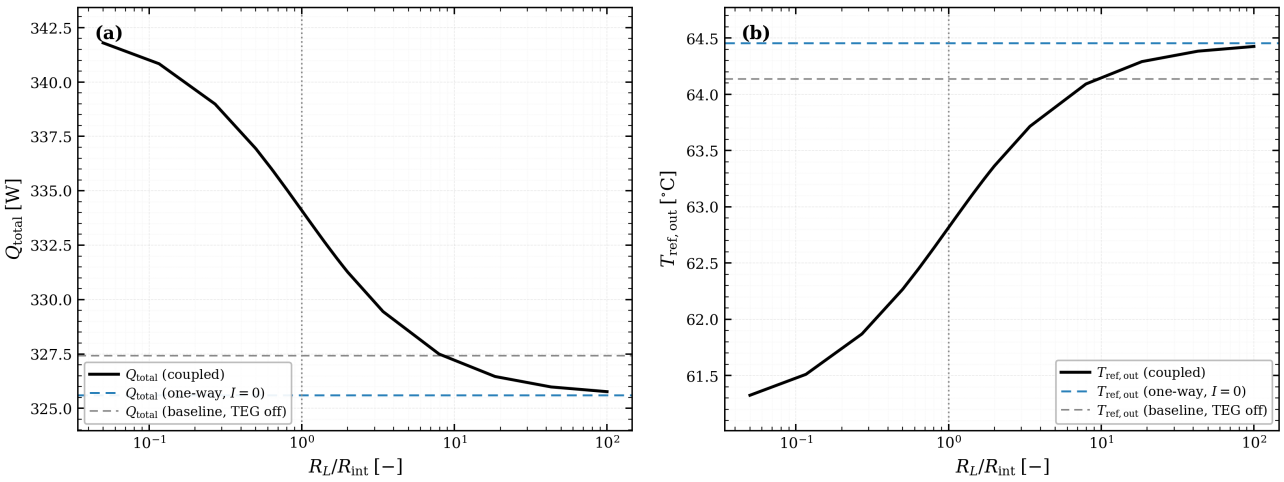

Figure 5: Impact of electro-thermal coupling on condenser performance: (a) total heat transfer rate; (b) outlet refrigerant temperature.

At low load resistance, the electrical current is higher and the coupled solution departs from the passive thermoelectric limit. As the load resistance increases, the current progressively vanishes and the solution approaches the open-circuit case. Compared with the passive thermoelectric configuration ((I = 0)), the electrical current modifies the local wall boundary conditions through Peltier and Joule effects, increasing the hot-side heat absorption and partially compensating for the thermal resistance introduced by the thermoelectric wall. Nevertheless, under the investigated operating conditions, the coupled TTEG configuration still exhibits a lower overall heat-transfer rate than the baseline metal-wall condenser without thermoelectric integration.
Although the generated electrical power remains negligible compared with the total heat duty, the results show that local electro-thermal feedback can measurably alter global condenser performance.

5.4. Synthesis of electro-thermal behaviour

The results provide a consistent physical interpretation of thermoelectric-assisted condensation. While the overall condenser behaviour remains dominated by phase-change heat transfer, the thermoelectric wall modifies the local thermal transport through both passive and active mechanisms.
Under open-circuit conditions, the thermoelectric wall introduces an additional thermal resistance that reduces the local heat-transfer rate and delays condensation. When bidirectional coupling is activated, the electrical current generates a load-dependent electro-thermal feedback through Peltier heat transport and Joule dissipation. Although the electrical power output remains small compared with the condenser heat duty, these effects partially compensate for the passive thermal penalty and produce measurable changes in condensation length, outlet temperature, and total heat-transfer rate.
The maximum electrical power is obtained near the expected matched-load condition, $R_L \approx R_{\text{int}}$, confirming the internal consistency of the coupled formulation. The results therefore demonstrate that even relatively small levels of thermoelectric power generation can influence the local thermal behaviour of a two-phase condenser through electro-thermal coupling.

6. Conclusions

A coupled thermo-electric model has been developed to analyse the interaction between two-phase condensation and transverse thermoelectric power generation in a concentric condenser. The framework combines segment-resolved thermo-hydraulic calculations with a load-dependent thermoelec-

tric formulation, enabling bidirectional electro-thermal coupling between the thermal and electrical domains.

The results show that the thermoelectric wall introduces an additional thermal resistance under open-circuit conditions, while electrical current generation partially compensates for this penalty through Peltier-driven heat transport. The coupled simulations reproduce the expected maximum-power condition near $R_L \approx R_{\text{int}}$ and demonstrate that electro-thermal feedback can produce measurable variations in condenser performance, despite the relatively small electrical power generated under the investigated conditions.

Overall, the proposed framework provides a physically consistent basis for analysing thermoelectric-assisted condensers and identifying operating regimes where electro-thermal coupling becomes significant. Future work will focus on larger temperature gradients, improved thermoelectric materials, and experimental validation of the coupled condenser configuration.

Acknowledgments

This work was supported by the MultithermEX project, funded by the Walloon Region under the Win2Wal program, involving collaboration between UCLouvain and University of Liège, with industrial participation from Calyos.

Nomenclature

Latin symbols

a	metal volume fraction	$-$
C	heat capacity rate	W/K
h	specific enthalpy	J/kg
I	electrical current	A
G	thermal conductance	W/K
$\dot{m}$	mass flow rate	kg/s
NTU	number of transfer units	$-$
Nu	Nusselt number	$-$
P	electrical power	W
Pr	Prandtl number	$-$
q	segment heat duty	W
Q	heat transfer rate	W
Re	Reynolds number	$-$
R	resistance	Ω, K/W
S	Seebeck coefficient	V/K
UA	thermal conductance	W/K
V	electrical voltage	V
x	vapour quality	$-$

Greek symbols

ε	heat exchanger effectiveness	$-$
ΔP	pressure drop	Pa
Δz	segment length	m
θ	laminate inclination angle	deg
k_{eff}	effective thermal conductivity	W/(m·K)
σ_{eff}	effective electrical conductivity	S/m

Subscripts

c	cold side
el	electrical
th	conductive thermal
eff	effective property
h	hot side
int	internal
$load$	external load
oc	open circuit
ref	refrigerant side
$water$	cooling water side

References

[1] Siedel B., Sartre V., Lefèvre F. *Literature review: Steady-state modelling of loop heat pipes*. Applied Thermal Engineering 2015;75:709–723. https://doi.org/10.1016/j.applthermaleng.2014.10.030

[2] He W., Zhang G., Zhang X., Ji J., Li G., Zhao X. *Recent development and application of thermoelectric generator and cooler*. Applied Energy 2015;143:1–25. https://doi.org/10.1016/j.apenergy.2014.12.075

[3] Zhao D., Tan G. *A review of thermoelectric cooling: Materials, modeling and applications*. Applied Thermal Engineering 2014;66:15–24. https://doi.org/10.1016/j.applthermaleng.2014.01.074

[4] Remeli M.F., Tan L., Date A., Singh B., Akbarzadeh A. *Simultaneous power generation and heat recovery using a heat pipe assisted thermoelectric generator system*. Energy Conversion and Management 2015;91:110–119. https://doi.org/10.1016/j.enconman.2014.12.001

[5] Kuan W.K., Huang B.J. *Performance analysis of a thermoelectric generator integrated with a heat exchanger*. Energy Conversion and Management 2022;252:115096. https://doi.org/10.1016/j.enconman.2021.115096

[6] He W., Wang S., Yue L. *Enhanced thermoelectric performance of heat exchanger systems with integrated TEG modules*. Applied Energy 2019;237:626–639. https://doi.org/10.1016/j.apenergy.2019.01.050

[7] Meng F., Chen L., Sun F. *Thermoelectric generator for industrial waste heat recovery: A review*. Energy 2017;122:241–254. https://doi.org/10.1016/j.energy.2017.01.101

[8] Zhang X., Chau K.T., Chan C.C. *Thermoelectric generation from vehicle exhaust heat: Modeling and optimization*. Applied Energy 2020;262:114537. https://doi.org/10.1016/j.apenergy.2020.114537

[9] Kyarad A., Lengfellner H. *Transverse Peltier effect in tilted Pb–Bi_2Te_3 multilayer structures*. Applied Physics Letters 2006;89(19):192103. https://doi.org/10.1063/1.2385213

[10] Kanno T., Sakai A., Takahashi K., Omori T., Watanabe R. *Enhancement of transverse thermoelectric properties in tilted multilayer structures*. Applied Physics Letters 2009;94(6):061917. https://doi.org/10.1063/1.3077019

[11] Sakai A., Kanno T., Takahashi K., Tamaki H., Adachi H., Yamada Y. *Enhancement in performance of the tubular thermoelectric generator (TTEG)*. Journal of Electronic Materials 2013;42(7):1612–1616. https://doi.org/10.1007/s11664-012-2355-4

[12] Takahashi K., Kanno T., Sakai A., Tamaki H., Kusada H., Yamada Y. *Bifunctional thermoelectric tube made of tilted multilayer material as an alternative to standard heat exchangers*. Scientific Reports 2013;3:1501. https://doi.org/10.1038/srep01501

[13] Patil D.S., Arakerimath R.R., Walke P.V. *Thermoelectric materials and heat exchangers for power generation — a review*. Renewable and Sustainable Energy Reviews 2018;95:1–22. https://doi.org/10.1016/j.rser.2018.07.003

[14] Gnielinski V. *New equations for heat and mass transfer in turbulent pipe and channel flow*. International Chemical Engineering 1976;16(2):359–368.

[15] Shah M.M. *Heat transfer during condensation inside pipes: A comprehensive review*. International Journal of Heat and Mass Transfer 2021;165:120668. https://doi.org/10.1016/j.ijheatmasstransfer.2020.120668

[16] Zivi S.M. *Estimation of steady-state void fraction by means of the principle of minimum entropy production*. Journal of Heat Transfer 1964;86:247–252.

[17] Friedel L. *Improved friction pressure drop correlations for horizontal and vertical two-phase pipe flow*. European Two-Phase Flow Group Meeting, Paper E2, 1979.

[18] Incropera F.P., Dewitt D.P., Bergman T.L., Lavine A.S. *Fundamentals of Heat and Mass Transfer*, 6th ed. John Wiley & Sons, Hoboken, NJ, 2007.

[19] Bell I.H., Wronski J., Quoilin S., Lemort V. *Pure and pseudo-pure fluid thermophysical property evaluation and the open-source thermophysical property library CoolProp*. Industrial & Engineering Chemistry Research 2014;53(6):2498–2508. https://doi.org/10.1021/ie4033999